JOURNAL OF GEOPHYSICAL RESEARCH, VOL. 102, NO. D25, PAGES 29,849-29,866, DECEMBER 27, 1997

Analysis and validation of GPS/MET data in the neutral atmosphere

C. Rocken,[1,2] R. Anthes,[2] M. Exner,[2] D. Hunt,[2] S. Sokolovskiy,[3] R. Ware,[1,2]
M. Gorbunov,[3] W. Schreiner,[2] D. Feng,[4] B. Herman,[4] Y.-H. Kuo,[5] X. Zou[5]

Abstract. The Global Positioning System/Meteorology (GPS/MET) Program was established in 1993 by the University Corporation for Atmospheric Research (UCAR) to demonstrate active limb sounding of the Earth's atmosphere using the radio occultation technique. The demonstration system observes occulted GPS satellite signals received by a low Earth orbiting (LEO) satellite, MicroLab-1, launched April 3, 1995. The system can profile ionospheric electron density and neutral atmospheric properties. Neutral atmospheric refractivity, density, pressure, and temperature are derived at altitudes where the amount of water vapor is low. At lower altitudes, vertical profiles of density, pressure, and water vapor pressure can be derived from the GPS/MET refractivity profiles if temperature data from an independent source are available. This paper describes the GPS/MET data analysis procedures and validates GPS/MET data with statistics and illustrative case studies. We compare more than 1200 GPS/MET neutral atmosphere soundings to correlative data from operational global weather analyses, radiosondes, and the GOES, TOVS, UARS/MLS and HALOE orbiting atmospheric sensors. Even though many GPS/MET soundings currently fail to penetrate the lowest 5 km of the troposphere in the presence of significant water vapor, our results demonstrate 1°C mean temperature agreement with the best correlative data sets between 1 and 40 km. This and the fact that GPS/MET observations are all-weather and self-calibrating suggests that radio occultation technology has the potential to make a strong contribution to a global observing system supporting weather prediction and weather and climate research.

1. Introduction

Radio occultation is a technique for sounding the structure of planetary atmospheres that was pioneered by groups at the Jet Propulsion Laboratory (JPL) and Stanford University over 30 years ago [*Fjeldbo et al.*, 1971]. The Global Positioning System/Meteorology (GPS/MET) experiment uses radio occultation observations of GPS satellites to obtain vertical profiles of electron density in the ionosphere; refractivity, density, pressure, and temperature in the stratosphere and upper troposphere; and refractivity, density, pressure and water vapor pressure in the lower troposphere.

The GPS/MET instrument orbits the Earth aboard the MicroLab-1 satellite at an altitude of ~730 km with a period of 100 min. Occultations occur as the instrument sets below Earth's horizon relative to any of the 24 GPS satellites, which orbit Earth at ~20,200 km altitude twice a day and broadcast signals continuously at 1.2 GHz (L2) and 1.6 GHz (L1). Approximately 250 such setting occultations occur each day (the GPS/MET instrument is capable of tracking rising and setting occultations, but not simultaneously). However, because of gaps in the ground tracking network and memory limitations on board MicroLab-1, the GPS/MET instrument collects only about 150 soundings per day under optimum conditions.

When the GPS/MET instrument tracks a GPS satellite as it is occulted by Earth's atmosphere, the arrival time of the GPS signal at the instrument is delayed because of refractive bending and slowing of the signal. The GPS/MET instrument records the carrier phase change on the GPS to low Earth orbiting (LEO) microwave links 50 times per second with millimeter-scale precision. After removal of the nominal carrier frequency, the phase on these links changes for three reasons: (1) relative motion of the LEO and GPS satellites, (2) drift of the clocks in the GPS transmitters and receivers, and (3) refractive bending and propagation velocity changes in the ionosphere and neutral atmosphere. As described in more detail below, the GPS/MET data analysis algorithm removes effects (1) and (2) from the data and computes the Doppler shift due to the atmosphere ("excess Doppler"). From this excess Doppler, atmospheric refractivity profiles can be computed as a function of ray tangent height above the surface. For neutral atmospheric soundings the GPS/MET instrument measures the excess Doppler every 20 ms (50 Hz) during the 80-s period of a typical occultation. This results in about 4000 measurements for each profile, which typically starts at 100 km for the neutral atmosphere and ends near the surface for setting occultations.

[1] University NAVSTAR Consortium, Boulder, Colorado

[2] University Corporation for Atmospheric Research, Boulder, Colorado

[3] Russian Institute of Atmospheric Physics, Moscow

[4] Department of Atmospheric Sciences, University of Arizona, Tucson, Arizona

[5] National Center for Atmospheric Research, Boulder, Colorado

Paper number 97JD02400
0148-0227/97/97JD-02400$09.00

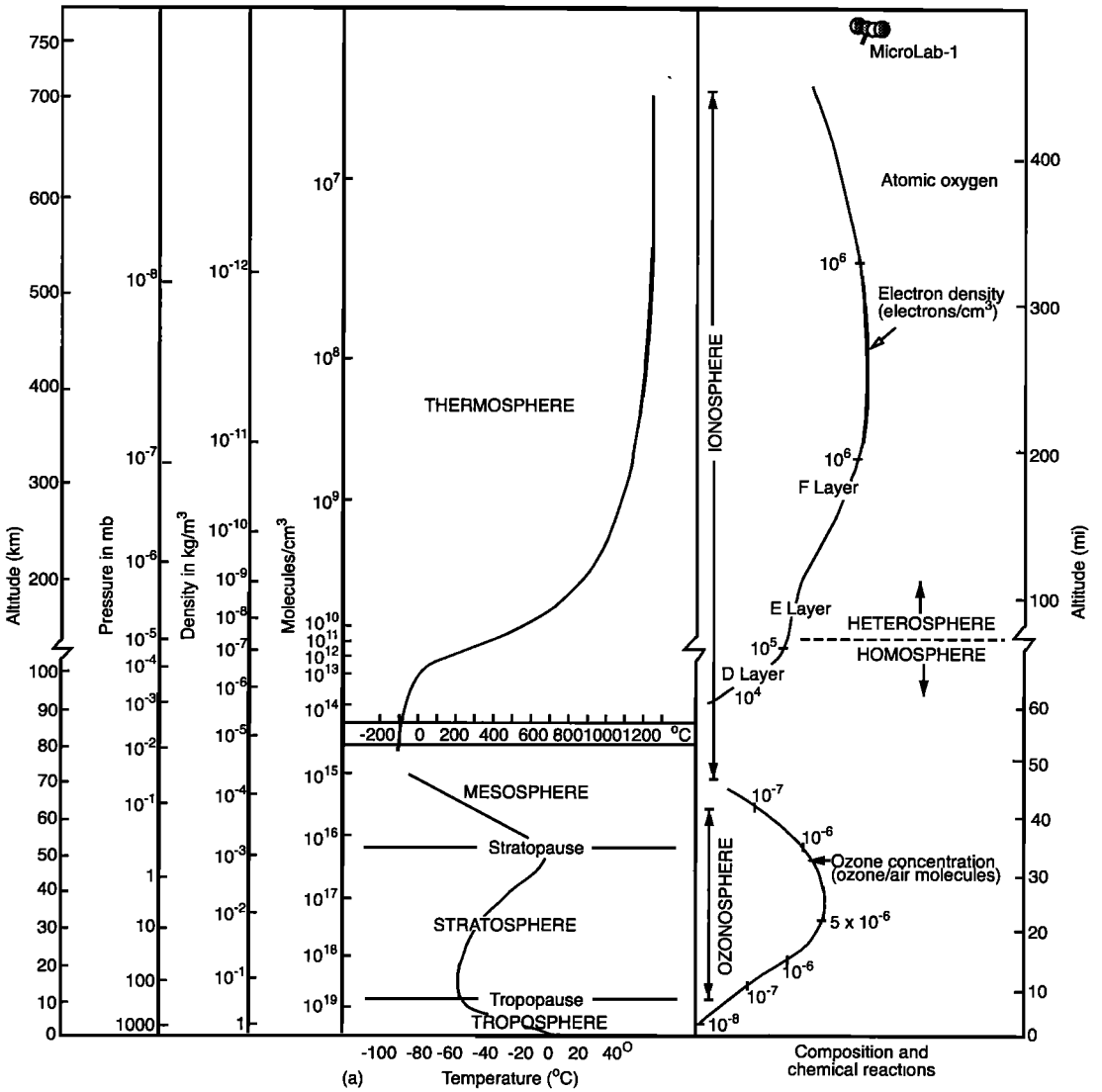

Figure 1. The mean vertical structure of Earth's atmosphere showing the orbit altitude of MicroLab-I and regions where profiles can be obtained from GPS/MET limb soundings. In addition, ionospheric total electron content can be observed by GPS/MET along ray paths from GPS satellites at all altitudes (adapted from Anthes [1997]).

Although the sampling rate corresponds to several tens of meters, the current instrument's vertical resolution is limited by several factors: system measurement noise, diffraction, and horizontal atmospheric inhomogeneity. The last two factors are dominant and limit the vertical resolution to approximately 1.5 km in the stratosphere to 0.1-0.5 km in the lower troposphere [*Melbourne et al.*, 1994].

The horizontal resolution is about 300 km along the GPS ray path and about 1.5 km perpendicular to the path. The predicted maximum accuracy of a GPS radio occultation system is 1°C or better for a height range of 5 to 40 km [*Melbourne et al.*, 1994; *Gorbunov and Sokolovskiy*, 1993]. Earlier studies have shown that GPS/MET comes close to performing as well as this prediction. Comparisons of 11 representative temperature profiles derived from GPS/MET data with nearby radiosonde and global analyses of temperatures are described by *Ware et al.* [1996]. *Kursinski et al.* [1996] provide a statistical comparison of about 100 GPS/MET temperature profiles with global analyses between 10 and 25 km, where water vapor effects are minimal.

GPS/MET is an all-weather system with global coverage, practically unaffected by clouds, precipitation, and aerosols. The system has the capability for seamless soundings of refractivity from orbit altitude to near the surface including top and bottom sounding of ionospheric electron densities (Figure 1). The system does not depend on radiosondes (except indirectly for water vapor retrievals as described below), and the instruments do not require calibration beyond the analysis described in this paper, thus providing long term stability important for climate variability studies.

To evaluate the radio occultation method for operational and research use, the experimental GPS/MET data must be carefully compared with data from independent sources. In this paper we compare more than 1200 GPS/MET neutral atmosphere soundings to correlative data sets including operational global analyses from the National Centers for Environmental Prediction (NCEP) and the European Centre for Medium-Range Weather Forecasting (ECMWF), radiosonde data, and data from the sounder on the Geostationary Operational Environmental Satellite (GOES), the Television Infrared Observation System (TIROS) Operational

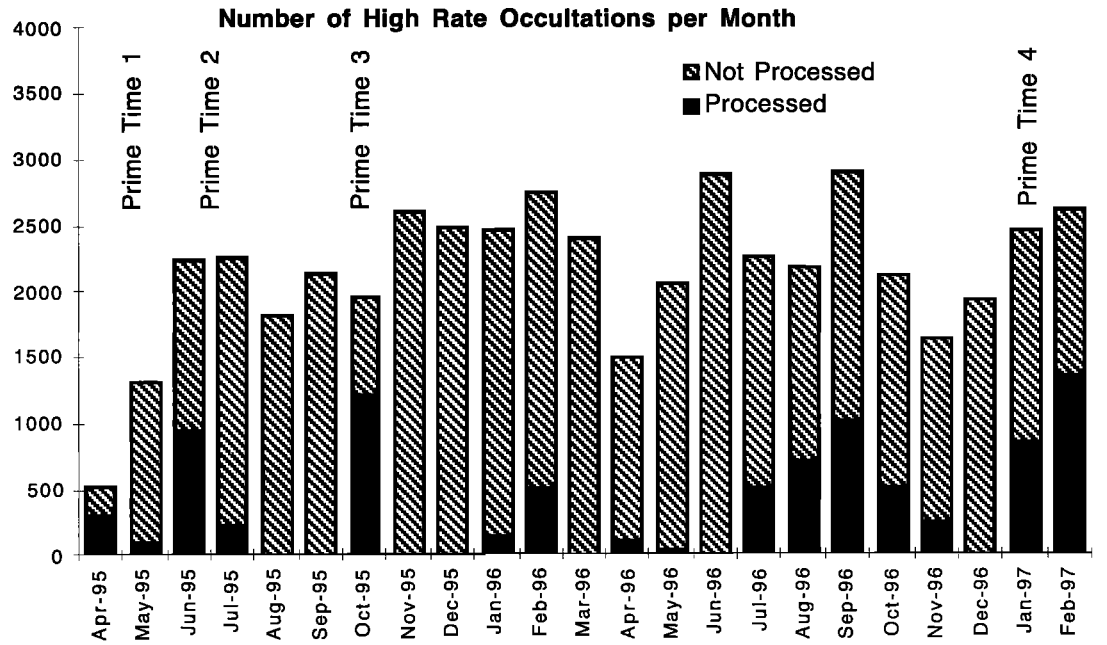

Figure 2. The number of GPS/MET occultations collected through February 1997. The number fluctuates depending on the geometric orientation of MicroLab-1, changes in satellite firmware, whether or not high-altitude ionospheric data are being collected, relative power and data telemetry demands, and the health of the satellite and ground tracking and telemetry systems. The number of occultations is limited to approximately 150 per day because only setting occultations from GPS are collected and because of gaps in the ground tracking network.

Vertical Sounder (TOVS), the Halogen Occultation Experiment (HALOE), and the Microwave Limb Sounder (MLS) instruments.

Section 2 summarizes GPS/MET data collected to date, describes data processing, the retrieval of water vapor profiles from GPS/MET refractivity profiles and auxiliary temperature data, ionospheric correction techniques, and discusses the vertical and horizontal resolution of GPS/MET data. Section 3 provides a description of the correlative data sets. Section 4 presents two illustrative examples of GPS/MET profiles, to demonstrate the high vertical resolution of the tropopause and a retrieved water vapor profile. In section 5 we compare correlative data sets with each other and with the GPS/MET data. Section 6 discusses the statistical comparisons and the difficulties interpreting data collected close to the Earth's surface with the proof-of-concept instrument. Section 7 summarizes our results and discusses scientific uses of the data.

2. GPS/MET Data and Analysis

Here we summarize the experimental data and the occultation data analysis algorithms with emphasis on recent developments that have not been previously described in the literature.

2.1. Available GPS/MET Data

Figure 2 displays the number of occultations that were collected between April 1995 and February 1997. It can be seen that to date we have processed only a fraction of the roughly 70,000 GPS/MET occultations that have been collected and archived. Our analysis has focused primarily on four "prime times". During prime times, anti-spoofing (A/S) encryption of the GPS signals was turned off, and MicroLab-1 was oriented so that GPS satellites were occulted in the aft or anti velocity direction toward Earth's limb.

When A/S is turned on, which is the normal operational mode for GPS, the GPS instrument on MicroLab-1 tracks the L1 carrier phase with the same precision as under A/S-off conditions. The L2 data, however, are significantly noisier and require modified data analysis techniques. We are currently testing new processing strategies for A/S-on occultations that rely on added smoothing of the "L1 minus L2" data. These techniques appear to be performing well for a significant fraction of our data at altitudes below 30 km, and we are confident that a large fraction of the A/S-on data in the GPS/MET database will be processed to high accuracy in the near future. This paper, however focuses on A/S-off results from prime time 3 (October 12 to 27, 1995).

2.2. GPS/MET Data Processing Description

All data are analyzed with original software developed by the UCAR GPS/MET team and commercial software. Data are processed through several steps, and intermediate products, referred to as Level 0, 1, 2, and 3 data, are created as described below.

The raw data transmitted by MicroLab-1 to the ground are called Level 0 data. After removal of packet communications headers and reformatting of the raw data, we generate Level 1 files containing GPS phase and amplitude time series. The next processing step removes phase changes due to satellite motion and clock drift from the data. To remove satellite motion, accurate GPS satellite and LEO positions and velocities are computed with the commercial precision orbit determination (POD) software "MicroCosm™." To remove clock errors, we form so-called double differences between observations of the occulted satellite and a nonocculted reference satellite [e.g., *Ware et al.*, 1996]. Both satel-

lites have to be observed simultaneously from LEO and from a GPS receiver on the ground. Six such reference ground stations are operated by JPL as part of the International GPS Service [*Neilan*, 1995].

After satellite motion and clock errors have been removed from the phase observations, the resulting Level 2 files contain the excess phase delay of the GPS signal due to the atmosphere and ionosphere. Each Level 2 file contains one occultation, typically 4000 records of dual-frequency (L1 and L2) excess phase and carrier amplitude. Level 2 files also contain the LEO and GPS satellite positions and velocities that define the geometry of the occultation, and are needed to compute signal bending and location of the ray tangent point.

Next, atmospheric profile information is extracted from the Level 2 files in the following steps, described in more detail in sections 2.2.1 through 2.2.3.

1. Filter L1 and L2 excess phase time series, perform diffraction correction of L1 excess phase in the lower troposphere and differentiation of L1 and L2 phase to yield excess Doppler.

2. Calculate L1 and L2 refractive bending angles from L1 and L2 excess Doppler.

3. Compute bending angles from which the ionospheric effects have been removed.

4. Optimize the observed bending angles at altitudes above 50 km, using a climatological model (mean atmospheric reference state) and occultation specific error statistics.

5. Apply the Abel inversion [*Phinney and Anderson*, 1968] of bending angle time series to compute refractivity profiles, under the assumption of local spherical symmetry.

6. Compute meteorological parameters from retrieved refractivity (using ancillary temperature data to retrieve water vapor in the lower troposphere).

Inversion of the Level 2 files results in profiles of atmospheric refractivity, density, pressure, temperature, and with ancillary temperature data, water vapor pressure. These Level 3 profiles are stored as a function of ray tangent point, longitude, latitude and altitude above the geoid. Note that GPS/MET atmospheric profiles, including pressure, are an independent function of geometric height, an important difference from the correlative data, which compute geopotential height from pressure observations.

2.2.1. Phase filtering, diffraction correction, and calculation of bending angles. Level 2 excess phase observations are low-pass filtered to reduce noise, and its effect on subsequent nonlinear processing steps like the Abel transform. The cutoff frequency of the filter is tuned to pass phase variations corresponding to vertical scales of 2 to 3 km in the stratosphere and approximately 200 m in the lower troposphere.

Bending angles are computed from the excess Doppler, based on the geometrical relationship of the wave vectors (e.g., ray directions) and the velocity vectors of occulted GPS and LEO satellites. This relationship is only valid for propagation of one ray, however. The complicated structure of the humidity field in the lower troposphere can produce strong refractivity gradients that can cause multipath propagation. The severity of multipath propagation depends on the observation geometry. The greater the distance from the ray tangent point to the LEO instrument, the stronger are multipath effects caused by atmospheric refractivity gradients.

The electromagnetic field affected by multipath propagation undergoes strong oscillations due to interference of different rays received by the LEO instrument. Numerical simulations with a thin phase screen model indicate that geometrical optics often fails to describe the resulting field, especially in the vicinity of caustics, i.e. surfaces where focusing takes place [*Gorbunov et al.*, 1996]. Standard algorithms for the derivation of bending angles from GPS excess Doppler result in ambiguities of the bending angle as a function of height. Such ambiguities cause the Abel transform technique to fail and must be avoided. In the past we have smoothed the data to solve this problem, but for the inversions in this study, a new diffraction correction technique was implemented [*Karayel and Hinson*, 1997; M.E. Gorbunov and A.S. Gurvich, Microlab-1 experiment: Multipath effects in the troposphere, submitted to *Journal of Geophysical Research*, 1997; hereinafter referred to as submitted paper].

The amplitude and phase measurements along the LEO orbit allow us to formulate the boundary problem for the Helmholtz equation describing the complex amplitude of the electromagnetic field in the occultation plane. Using the solution of the boundary problem in a vacuum, we reconstruct the ray structure of the received field close to the area which causes the multipath, and thus "disentangle" the multiple rays arriving simultaneously at the receiver.

Thus, by recalculating the field for an auxiliary plane located closer to the ray tangent point, but outside of the neutral atmosphere, we can greatly reduce the effect of multipath propagation. Our experience with the diffraction correction algorithm showed that almost all bending angle ambiguities were eliminated without the need for further smoothing.

In summary, application of the diffraction correction algorithm results in elimination of bending angle ambiguities, in improved vertical resolution, and it can affect temperature measurements in the lower troposphere by several degrees.

2.2.2. Ionospheric correction and optimization of bending angles. Calculation and removal of bending in the ionosphere is required for GPS/MET soundings of the neutral atmosphere. We apply a model independent ionospheric correction by forming a linear combination of L1 and L2 bending angles [*Vorob'ev and Krasil'nikova*, 1994]. This correction, however, is not applied in the lower troposphere because the L2 data (which are transmitted from the GPS satellite at about -6dB lower power levels than L1) become very noisy in this region. Instead, an extrapolated difference of L1 and L2 bending angles is used for ionospheric correction during the last few seconds of each occultation.

Analysis of our data between 60 and 80 km (above neutral bending, but below the ionospheric E layer) shows that noise-like fluctuations, presumably due to ionospheric turbulence along the ray path, are not fully removed by the ionospheric correction. The magnitude of this residual ionospheric noise is different for each occultation, but for most occultations, it clearly dominates over measurement noise.

For A/S-off data, the mean magnitude of this residual bending angle noise is about 1.5×10^{-6} radians. Under current ionospheric conditions this noise is mostly random and it is larger than bending due to the neutral atmosphere above 65 to 70 km. How best to deal with this noise depends on the final goal of the retrieval. For climate monitoring and research, one could average a large number of occultations to suppress the high frequency components of the noise. The resulting averaged bending angles can then be compared to bending angles calculated from climate models, or used directly for monitoring climate change and variability.

If the GPS/MET data are to be used for weather prediction, then the difference between the individual sounding and a mean atmospheric state is of interest. In this case, we may initialize the sounding at some high altitude (e.g., 100 km) with data from a reference atmosphere to minimize downward propagation of errors when applying the Abel inversion.

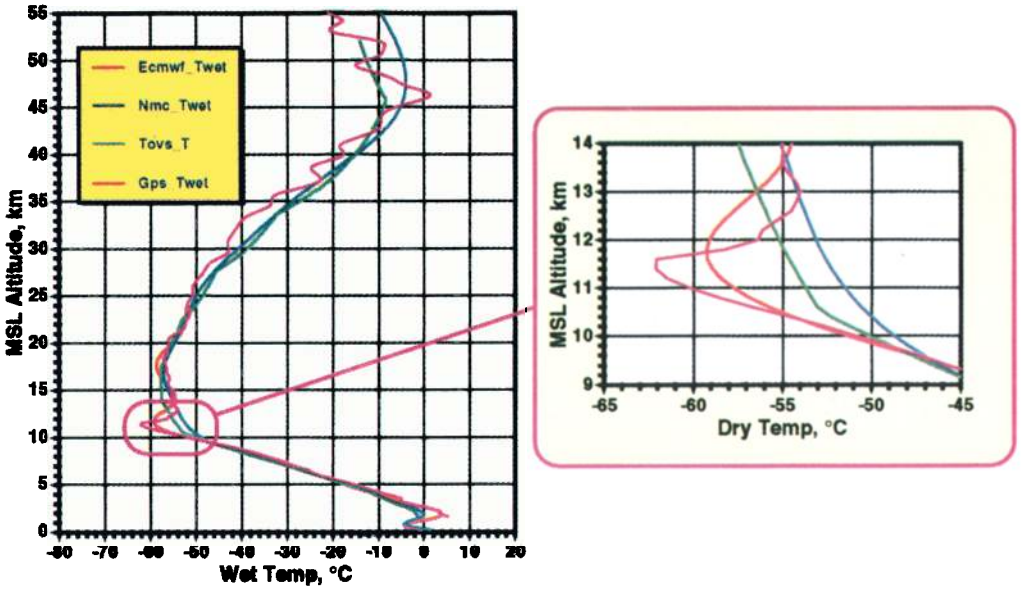

Plate 1. Dry temperature retrieval from GPS/MET occultation 0136 observed at 17:24 UTC on October 21, 1995, at 48°S/159°W. Sharp resolution of the tropopause is seen in the GPS/MET profile, compared to NCEP, ECMWF, and TOVS profiles.

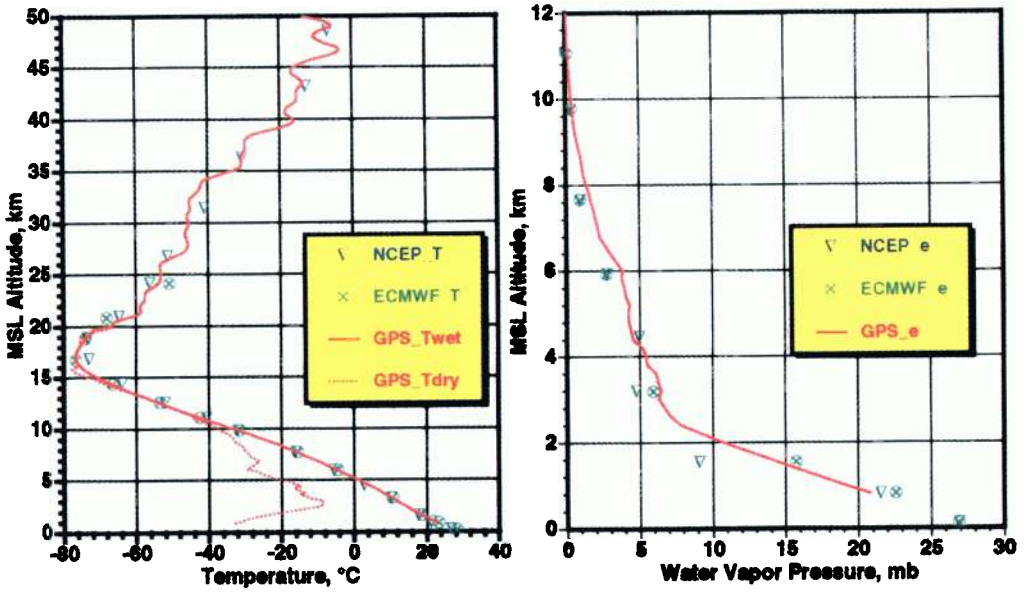

Plate 2. Profiles from GPS/MET occultation 0066, observed at 1140 UTC on June 22, 1995, at 9°S/172°W. Water vapor pressure reaches 20 mbar at ~800 m above the surface.

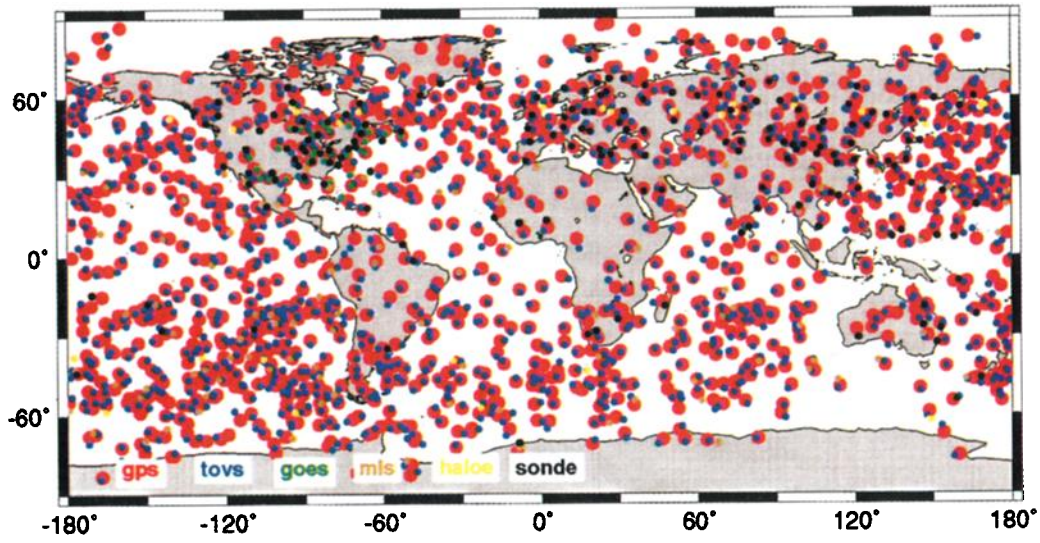

Plate 3. Locations of the GPS/MET soundings (large red dots) and the correlative data that were compared during Prime Time 3.

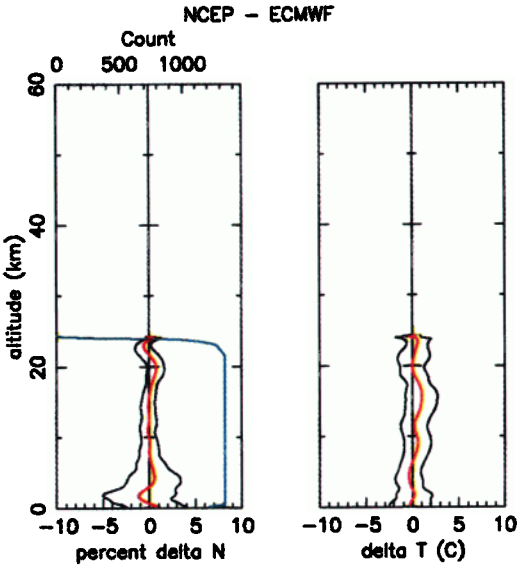

Plate 4. Comparison of NCEP and ECMWF profiles at the locations of GPS/MET occultations during Prime Time 3. The left panel compares refractivity (N) and the right panel compares temperature (T). The blue line in the left panel shows the number of observations at each altitude used for the comparison, according to the scale on top of the graph. Each plot shows average differences in red, surrounded in black by the 1-sigma standard deviation about the mean. The standard error of the mean is shown by short green horizontal lines centered on the average difference curves.

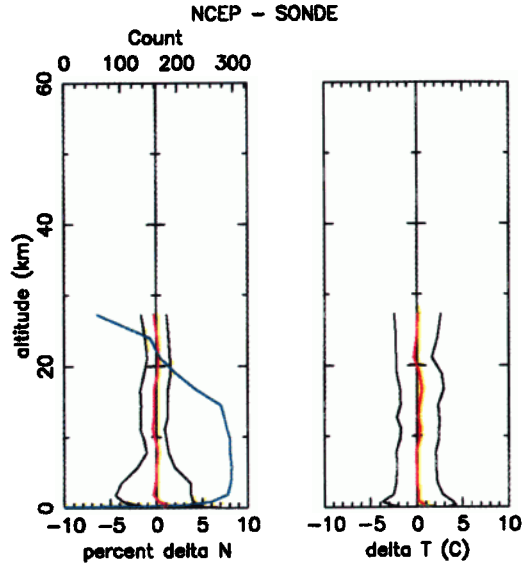

Plate 5. Comparison of NCEP and radiosonde refractivity and temperature at GPS/MET occultation locations and times.

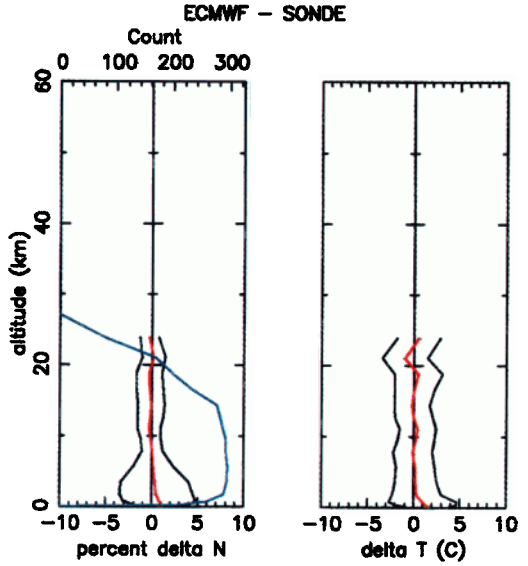

Plate 6. Comparison of ECMWF and radiosonde refractivity and temperature profiles at GPS/MET occultation locations and times.

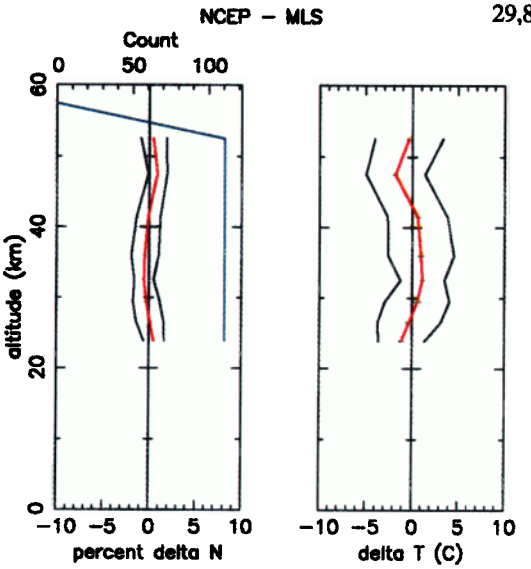

Plate 7. Comparison of NCEP and MLS refractivity and temperature profiles at GPS/MET occultation locations and times.

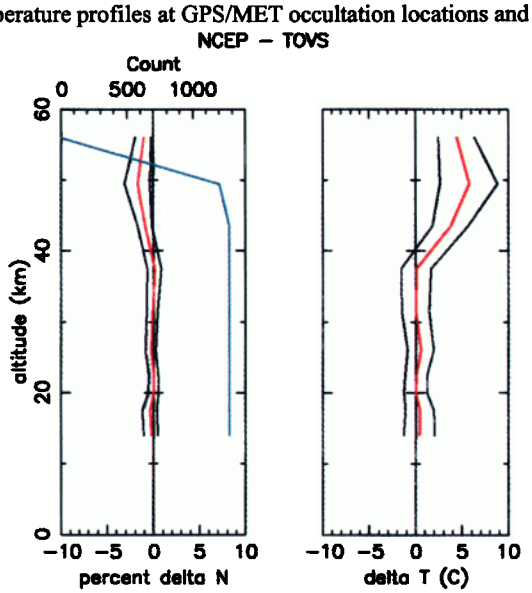

Plate 8. Comparison of NCEP and TOVS refractivity and temperature profiles at GPS/MET occultation locations and times.

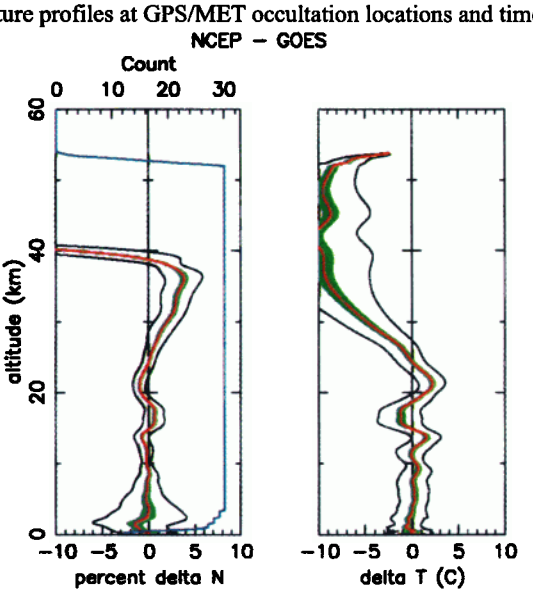

Plate 9. Comparison of NCEP and GOES refractivity and temperature profiles at GPS/MET occultation locations and times.

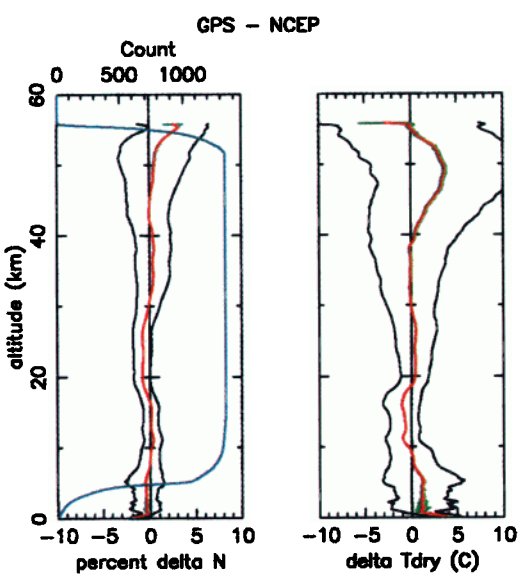

Plate 10. Comparison of GPS/MET and NCEP refractivity and dry temperature profiles.

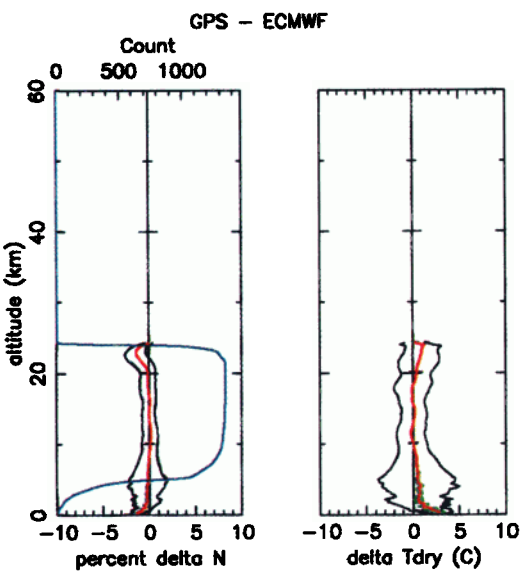

Plate 11. Comparison of GPS/MET and ECMWF refractivity and dry temperature profiles.

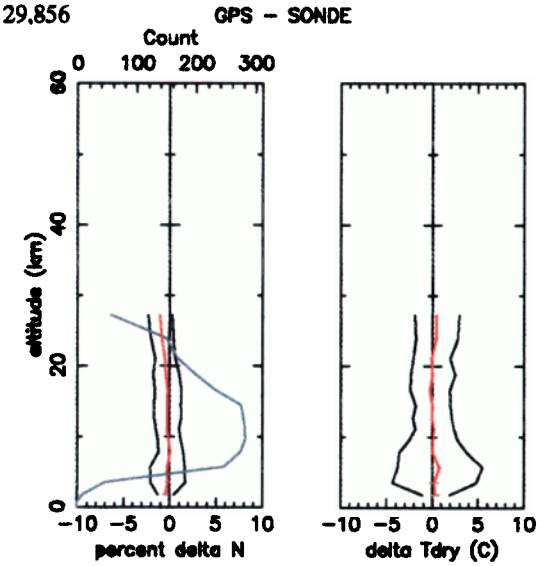

Plate 12. Comparison of GPS/MET and radiosonde refractivity and dry temperature profiles.

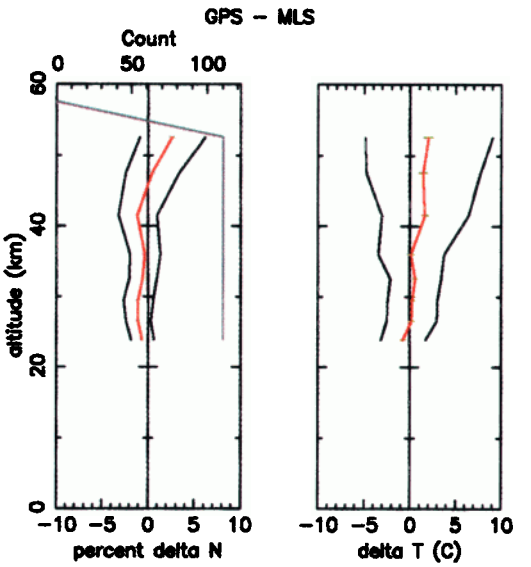

Plate 13. Comparison of GPS/MET and MLS refractivity and temperature profiles.

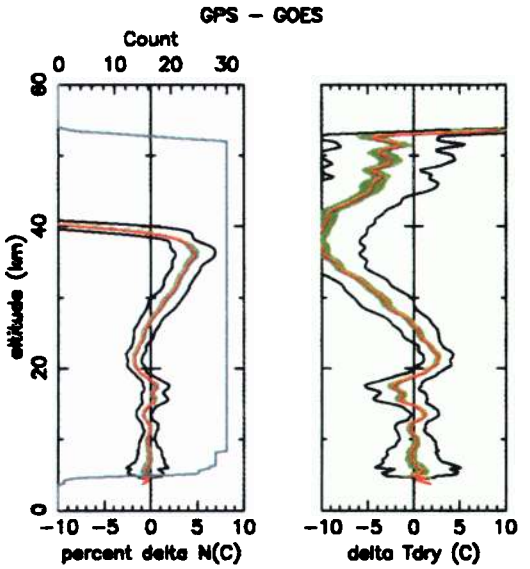

Plate 14. Comparison of GPS/MET and GOES refractivity and dry temperature profiles.

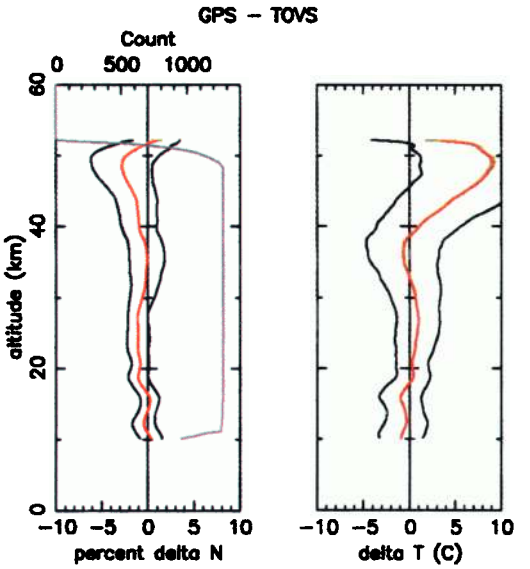

Plate 15. Comparison of GPS/MET and TOVS refractivity and temperature profiles.

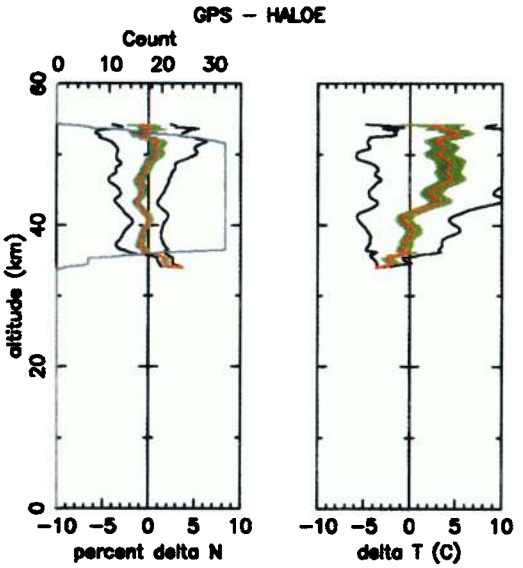

Plate 16. Comparison of GPS/MET and HALOE refractivity and temperature profiles.

Traditional "initialization" of the Abel inversion substitutes climatological data for observational data above the highest altitude for which observations become less reliable than an estimate based on climatology. We improve upon this approach by computing the most likely bending angle profiles from the observations in combination with climatology, using a weighting function defined by their respective error statistics. This statistical optimization approach results in a smooth transition from the mean atmospheric state at high altitudes to observations at lower altitudes, minimizing error propagation downward. The CIRA-86 zonal-mean global climatological model (CIRA, 1986, 1988, CIRA-86, 1990) with 10° latitudinal and 1 month temporal increments is used for the statistical optimization. Weighting functions are calculated for each occultation based on observation noise in the 60 to 80 km range. The weighting function is equal to 0.5 when the observation noise equals the expected standard deviation of the atmospheric state from the mean reference state. This happens typically at an altitude of 50 km. Thus the GPS/MET results presented in this study are influenced significantly by climatology above 50 km. Below an altitude of approximately 40 km, climatology is typically weighted so low that it has no material influence.

It should be emphasized that statistical optimization cannot improve the quality of the observational data at high altitudes. The technique substitutes the statistically most likely vector for the observational vector. Thus it minimizes error propagation downwards to those elevations where GPS/MET data have relatively high signal to noise, and are potentially most valuable for weather prediction. Statistical optimization was first introduced by *Sokolovskiy and Hunt* [1996], and has also been implemented by *Hocke* [1997].

2.2.3. Calculation of atmospheric pressure, temperature, and water vapor profiles from GPS/MET refractivities. After accounting for ionospheric bending as described above, the refractivity (N) is related to pressure (P in mbar), temperature (T in K), and water vapor pressure (e in mbar) by the equation [*Smith and Weintraub*, 1953; *Thayer*, 1974]

$$N = 77.6\frac{P}{T} + 3.73 \times 10^5 \frac{e}{T^2} \quad (1)$$

Previous publications [e.g., *Melbourne et al.*, 1994; *Ware et al.*, 1996] explain how refractivity profiles can be converted to profiles of pressure and temperature under the assumption of hydrostatic equilibrium and zero water vapor pressure. This conversion yields accurate temperature and pressure profiles above the moist layers of the troposphere (typically 5 to 10 km, depending on season and latitude).

Water vapor pressure can be derived from the retrieved GPS/MET refractivity, using equation (1), if pressure and temperature are known. Because pressure, temperature and water vapor are related through the hydrostatic equation and the equation of state for moist air, water vapor pressure can be derived from refractivity if either pressure or temperature are independently known. In this case a simple recursive algorithm may be used to calculate T, P, and e from N and T or from N and P alone, starting at some upper level where e=0 and integrating downward. The water vapor profiles presented in this paper were computed in this way from GPS/MET refractivity and NCEP analysis temperature.

2.3. Vertical and Horizontal Resolution of GPS/MET

As stated in the introduction, the vertical resolution of the current GPS/MET instrument is limited by diffraction and atmospheric inhomogeneities along the ray path. *Melbourne et al.* [1994] show that the size of the first Fresnel zone, and therefore the vertical resolution, ranges from 0.1-0.5 km in the troposphere to 1.5 km in the stratosphere. Diffraction correction, as applied in our analysis, allows improvement of the vertical resolution beyond the Fresnel zone limit, based on synthetic aperture principles [M.E. Gorbunov and A.S. Gurvich, submitted paper, 1997; *Karayel and Hinson*, 1997]. The level of this improvement, however, is difficult to quantify because of the effects due to horizontal atmospheric inhomogeneities.

As noted above, we assume locally spherical symmetry in the atmosphere to apply the Abel inversion. Thus, horizontal gradients in refractivity result in errors in the inversion. Based on the approximation of local spherical symmetry, this technique is incapable of resolving inhomogeneities with small horizontal scales. Refractivity perturbations located along the sounding ray perturb the reconstructed refractivity profile at the ray tangent point. Errors resulting from the nonsphericity of the atmosphere can only approximately be interpreted as horizontal averaging. More precisely they are related through complicated functionals that depend on the ratio of vertical to horizontal refractivity inhomogeneity scales [*Gorbunov and Sokolovskiy*, 1993].

Usually the characteristic horizontal resolution is estimated to be 300 km, which is the length of that part of a ray where more than half of the neutral atmospheric bending occurs. However, numerical simulations with a model of an idealized atmospheric front [*Gurvich and Sokolovskiy*, 1985] showed that the horizontal resolution can be reduced to 50-100 km in the case of a front with a large slope. In general, the smaller the vertical scale of a localized inhomogeneity, the better its horizontal structure can be resolved. *Kuo et al.* [1997] show that GPS/MET soundings can resolve the temperature structure of upper level atmospheric fronts with an accuracy and resolution comparable to radiosondes.

Simulations with the ECHAM3 Atmospheric General Circulation Model [*Deutsches Klimarechenzentrum*, 1994] showed that rms temperature errors of the Abel inversion due to horizontal inhomogeneities are less than 0.5°C in the 10 to 30 km altitude range. These errors can increase significantly below 10 km, even with field reconstruction with data from a system of 18 GPS and 100 LEO satellites. Errors result mainly from the highly variable horizontal structure of the humidity field that cannot be resolved even with GPS/MET soundings of 200 km spacing [*Gorbunov et al.*, 1996].

It must be emphasized, however, that the errors due to the nonsphericity of the atmosphere are not inherent in the GPS/MET limb sounding method. They are only the result of using the Abel inversion technique. Application of this technique is useful for the current proof-of-concept experiment. However, for operational use, four dimensional data assimilation techniques, with direct assimilation of bending angles [*Eyre*, 1994] can be used. This will allow more accurate and effective use of the GPS/MET observations and their error covariance matrices, by taking into account a priori information such as the first guess of the numerical weather prediction model and the covariance of the relevant variables.

3. Correlative Data

This section briefly describes the correlative data and global analysis fields against which the GPS/MET observations are evaluated.

3.1. Radiosondes

Radiosondes have been the backbone of the global upper air observing system since the 1940s. In 1991 there were more than 1000 radiosonde stations operated by 92 nations using 39 different types of radiosondes [*NOAA*, 1992]. Under ideal conditions and with careful calibration, radiosonde temperatures are accurate to within 0.5°C and relative humidities are accurate to within a few percent, except at very low temperatures or very high or low relative humidities [*Shea et al.*, 1994; *Ahnert*, 1991; *Luers and Eskridge*, 1995]. Under operational conditions, relative humidity errors are considerably greater than a few percent.

Radiosondes provide data from near the surface to an altitude of about 20 to 30 km. Because of pressure errors and resulting height errors, temperature accuracy is degraded in the upper troposphere and stratosphere, with typical errors of 1°C above 250 mbar (10.5 km) increasing to as large as 4°C at 10 mb (31 km) [*Nash and Schmidlin*, 1987].

Radiosondes produce soundings with high vertical resolution, resolving features with vertical scales of a few tens of meters. However, the coverage of radiosondes is uneven over Earth, with very few stations in oceanic regions. The temporal frequency is also fairly low (12 hr at best, with many countries taking only one observation per day) and they suffer from substantial changes in instrumentation with time [*Schwartz and Doswell*, 1991]. For humidity, complicating factors have been the use of low quality sensors, changes in the type of humidity sensing element, and changes in reporting procedures at low humidity [*Elliott and Gaffen*, 1991].

Nevertheless, radiosondes are the most accurate source of data influencing the global upper atmosphere analyses produced by operational centers such as NCEP and ECMWF (R. McPherson and E. Kalnay, personal communication, 1996). They also have a major impact on the GOES and TOVS radiometric soundings through the calibration and tuning of these satellite retrievals, and in their influence on the model first guess fields [*Menzel and Purdom*, 1994; *Smith et al.*, 1979].

3.2. Global Weather Analyses

We use the NCEP/NCAR reanalysis [*Kalnay et al.*, 1996] together with four pressure levels (5, 2, 1, 0.4 mbar) from the NCEP global stratospheric analysis for comparison with GPS/MET. The NCEP/NCAR reanalysis produces gridded data with 17 pressure levels ranging from 1000 mbar to 10 mbar. Horizontal and temporal resolution are 2.5° in longitude and latitude and 6 hours, respectively. We use geopotential heights, pressure, temperature and humidity from this data set. *Trenberth and Guillemot* [1996] evaluate the moisture fields in the NCEP/NCAR reanalysis and report significant negative bias in the water vapor fields in the tropics. The NCEP stratospheric analysis is a global, 24 hour analysis with eight pressure levels ranging from 70 mbar to 0.4 mbar. We use the top four levels to generate the combined NCEP comparison data set. The stratospheric analysis is divided into two grids, one for the Southern and one for the Northern hemisphere. Each is a 65 by 65 polar stereographic grid. Spatial interpolation for comparison with occultations is done separately for the reanalysis and stratospheric grids. The 1000 mbar to 20 mbar levels are used from the reanalysis and the 5 mbar to 0.4 mbar levels are used from the stratospheric data. The 10 mbar level occurs in both data sets and so the average value is used. Prior to comparison with other data sets we corrected the NCEP stratospheric temperatures according to adjustments published by *Gelman et al.* [1994].

The ECMWF TOGA Global Upper Air Analysis is a global, 12 hour, 2.5° latitude and longitude grid with 15 pressure levels ranging from 1000 mbar to 10 mbar. Data from the highest (10 mbar) level showed large differences (thought to be due to boundary conditions) from other correlative data and were not used. Thus the top level for ECMWF comparisons is 30 mbar.

3.3. GOES

GOES temperature profiles were computed at the University of Wisconsin at Madison. We compare GPS/MET data with profiles of temperature for clear atmospheric columns as retrieved from multispectral radiance observations by GOES-8 and GOES-9 [*Menzel and Purdom* 1994], using an extension of the algorithm described by *Hayden* [1988]. A retrieval is made for a region of 5 by 5 GOES sounder fields of view (fov), resulting in horizontal resolution of approximately 50 km for the retrieved products.

A cloud clearing procedure (C.M. Hayden et al., The cloud clearing for GOES product processing, submitted to *NOAA NESDIS Technical Reports*, 1997] is used to identify cloud contamination for each of the 25 fov. Retrievals are not attempted if fewer than 9 fov are found to be cloud free. Otherwise, radiances from all clear fov are averaged to enhance the signal to noise ratio. These averaged radiance measurements, representing the clear atmospheric column in the region, are then subject to a tuning process in order to remove biases [*Schmit*, 1996].

Finally, the cloud-cleared, regionally averaged, and bias-corrected radiance measurements are used for the simultaneous retrieval of temperature at 40 levels up to 0.1 mbar and humidity at 20 levels up to 100 mbar. The NCEP operational global model 12 hour forecast, interpolated to the observation time, is used as the first guess in the retrieval. Normally, the temperature retrieval is not very different from the first guess, and hence provides little new temperature information. In contrast, the humidity retrieval provides a significant amount of additional information about the atmospheric state.

3.4. TOVS

This study used TOVS data that were analyzed and provided to us by the National Environmental Satellite, Data, and Information Service (NESDIS). TOVS is composed of three radiometers: the High Resolution Infrared Sounder (HIRS/2), Microwave Sounder Unit (MSU) and Stratospheric Sounder Unit (SSU). The retrieval of temperature moisture and pressure from the radiance observations is described by *Smith et al.* [1979]. Cloud clearing was applied in the analysis of the TOVS data. Presently TOVS is the only data set that enters the NCEP stratospheric analysis.

3.5. UARS/MLS

Upper Atmosphere Research Satellite (UARS) MLS temperature measurements are useful for comparison with GPS/MET temperatures in the stratosphere. Temperatures and tangent point pressures (atmospheric pressures at the tangent height of the MLS radiometer field of view boresight) are retrieved from a 15-channel 63 GHz radiometer measuring oxygen microwave emissions from the stratosphere and mesosphere. E. Fishbein of the UARS/MLS team at JPL provided the most recent (Version 4) results. Version

4 MLS data are reported to provide useful temperatures from 0.46 to 46 mbar (approximately 25 to 55 km), which is an improvement over the minimum height of 22 mbar reported by *Fishbein et al.* [1996]. Accuracy estimates for the instrument range from 2.1°C at 22 mbar to 4.8°C at 0.46 mbar. The error increases to about 7°C at 46 mbar.

UARS/MLS temperatures are reported at seven pressure levels and the instrument points 90° relative to the orbit velocity. A full vertical scan takes about 65 s and is smeared over 400 km in the direction parallel to the satellite velocity of approximately 7 km/s. The profile is also "averaged" over a similar distance along the line of sight.

3.6. HALOE

HALOE on the UARS satellite is another instrument capable of temperature soundings [*Russell et al.*, 1993, 1994]. HALOE uses solar occultations to measure vertical profiles of O^3, HCl, HF, CH^4, H2O, NO, NO^2, aerosol extinction, and temperature as a function of pressure. The measurements have an instantaneous vertical field of view of 1.6 km at Earth's limb. Latitudinal coverage is from 80° S to 80° N.

The altitude for temperature measurements ranges from about 35 km to 80 km. Below 35 km, the HALOE temperature profile is identical to the NCEP analysis. Temperature precision is 2.5°C. A cold bias of 3 to 5°C within ±5 km of the stratopause has been reported. In the comparison height range covered by this paper, HALOE data were available for eight pressure levels between 4.6 and 0.3 mbar.

4. Individual Sounding Comparisons

Here we show examples of individual GPS/MET profiles to illustrate features not readily seen in the statistics which follow. We illustrate the high vertical resolution of the profile and show an example of how well atmospheric water vapor can be retrieved under favorable conditions.

4.1. Resolution of the Tropopause

Plate 1 compares a GPS/MET sounding with data from ECMWF and NCEP analyses interpolated to the time and location of the occultation, and with data from a nearby TOVS sounding.

The profile labeled T_{dry} in Plate 1 is "dry temperature", computed from equation (1) with $e = 0$. The calculation of dry temperatures is described in section 5. Plate 1 illustrates how GPS/MET resolves a sharp minimum temperature at the tropopause. The sharp feature is not resolved by the NCEP analysis or TOVS soundings, but it can be seen to some degree in the ECMWF profile.

4.2. Example Water Vapor Profile

The proof-of-concept GPS/MET instrument often has difficulty tracking the GPS signals close to the Earth's surface, especially in the presence of significant amounts of water vapor. Tracking problems close to Earth's surface are due in part to the relatively low gain antenna used for the GPS/MET proof-of-concept instrument. Future instruments will use higher gain directional antennas, providing higher carrier tracking loop bandwidth, more capable of tracking the rapidly fluctuating signals in the presence of refractivity gradients induced by water vapor variations.

Under ideal conditions, however, it is possible to retrieve useful data close to the surface with the current instrument as shown in Plate 2. In the left side of Plate 2, the actual temperature was estimated from the GPS/MET refractivity using the NCEP water vapor pressure as ancillary data; this estimate is labeled T_{wet}. NCEP analyzed temperatures were used to compute the water vapor profile from the GPS/MET refractivity profile.

GPS/MET refractivity measurements in moist layers provide valuable quantitative moisture information. It is likely that the calculation of water vapor pressure from observed values of refractivity and an independent estimate of temperature will be useful for climate studies and numerical weather prediction (NWP). The calculation of temperature from refractivity and an independent estimate of water vapor pressure is much more sensitive to small errors in water vapor pressure than is the calculation of water vapor pressure to small errors in temperature. *Ware et al.* [1996], for example, show that water vapor pressure near Earth's surface can be estimated within 0.5 mbar if the temperature is known to within 2°C. Temperature varies over larger horizontal and temporal scales in the atmosphere than does water vapor, is more easily measured, and hence is better resolved in operational analyses and model predictions. The present 6 hour forecast of temperature from a state-of-the-art numerical weather prediction model has a typical temperature error of 1°C [*Eyre*, 1994]. Thus, given the relatively high accuracy of existing temperature analyses and short-range forecasts together with the weak sensitivity of the water vapor pressure calculation to temperature errors, it should be possible to obtain useful global distributions of water vapor given global profiles of GPS/MET refractivity.

Plates 1 and 2 show GPS/MET temperature oscillations above approximately 30 km. Based on the relatively strong signal to noise ratio in the 10 to 40 km height range, it is likely that these fluctuations are real, perhaps caused by gravity waves [*Theon et al.*, 1967; *Vincent and Reid*, 1983; *Wilson et al.*, 1990]. At higher altitudes, residual ionospheric noise, which tends to dominate neutral atmospheric signal above 65 km, affects the retrievals and may contribute to the temperature oscillations. Other researchers observe similar GPS/MET temperature fluctuations [*Hocke*, 1997], but it has not been possible to verify whether GPS/MET is indeed resolving gravity waves in the 30 to 50 km range because none of the correlative data that we found had sufficient vertical and temporal resolution. Thus more research is required to determine the origin and accuracy of these oscillations.

5. Statistical Comparisons

5.1. Summary of Available Data

The statistical comparisons are based on GPS/MET data collected during the 16 day Prime Time 3 period from October 12 to 27, 1995. Plate 3 summarizes the distribution of all the data from this period.

For each variable compared (i.e., N, T, e) we compute and plot the ensemble mean differences, the standard deviation of the differences, and the standard error of the mean differences. If x_i is the difference between two like variables compared at a given altitude (i.e., $T_{GPS} - T_{NCEP}$), then the mean of the differences at this altitude

(or within an altitude layer in our binned comparisons) is given by

$$\bar{x} = \frac{\sum_{i=1}^{N} x_i}{N} \tag{2}$$

where N is the number of samples or comparison pairs available at a given altitude.

The standard deviation of the differences is

$$\sigma_x = \sqrt{\frac{1}{N}\sum_{i=1}^{N}(x_i - \bar{x})^2} \tag{3}$$

while the standard error of the mean differences is

$$\sigma_{\bar{x}} = \frac{\sigma_x}{\sqrt{N}} \tag{4}$$

It should be noted that everywhere in this paper where comparisons of the mean refractivity, temperature, and water vapor pressure are discussed, we speak about a comparison of the mean of the differences (equation (2)). Discussion of standard deviations always refers to standard deviation of the differences according to equation (3).

5.2. Comparison of Correlative Data

First, we compare correlative data at the locations and times of GPS/MET profiles to establish the degree of agreement among correlative data as a baseline against which to interpret the GPS/MET comparisons in section 5.3.

GPS/MET profiles are computed at their full 50 Hz sampling resolution and then interpolated to standard altitudes from 0 to 60 km in 200 m increments. Since the GPS/MET profiles have relatively high vertical sampling resolution, simple linear interpolation is sufficiently accurate for this step.

All comparisons are made as a function of altitude. Geometric altitude or height is the independent variable for GPS/MET data, while pressure is the independent variable for radiosonde, MLS, TOVS, HALOE, and GOES data. NCEP and ECMWF analysis data and radiosondes are provided with pressures and corresponding geopotential heights which are converted to geometric heights for comparison with GPS/MET.

For MLS, TOVS, GOES, and HALOE data, geometric heights are obtained by matching their pressure values with NCEP pressures and obtaining the corresponding NCEP geometric heights.

5.2.1. Comparison of NCEP and ECMWF analyses. To compare NCEP and ECMWF analysis data at the GPS/MET sounding times and locations, spatial and temporal interpolations of the gridded data are required. Two grids are selected, one from the model time immediately before, and one after the GPS/MET sounding. Latitude and longitude of the GPS/MET soundings are taken at 10 km height. A value for each model level of the analysis is determined by two-dimensional quadratic interpolation using the 16 grid point values surrounding the GPS/MET position. Taking these values for each level of the analysis yields a vertical comparison profile for the analysis times immediately before and after the occultation. These two profiles are then interpolated linearly to the time of the occultation. Plate 4 shows the statistical comparison of NCEP and ECMWF soundings at the locations of all occultations shown in Plate 3.

Plate 4 demonstrates that the mean difference between ECMWF and NCEP temperatures is generally less than 1°C with a standard deviation of 1 to 2°C. Average agreement in refractivity is better than 0.5% from 2 to 24 km, with a standard deviation of less than 1% above 10 km. The standard deviation increases to 4% in the lower troposphere; this increase is attributable to differences in water vapor distribution between the two analyses.

5.2.2. Comparison of NCEP and ECMWF analyses with radiosonde data. Next, NCEP and ECMWF data are compared to the radiosonde data which "match" the GPS/MET occultation times and locations. A match between GPS/MET and radiosondes, GOES, MLS, TOVS or HALOE is defined by a 4° latitude and longitude radius and a ±6 hour time window.

For the comparison with radiosonde data, NCEP and ECMWF profiles were interpolated to the matching occultation location and time, instead of the location and time of the radiosonde. This was done for all correlative data to show comparisons that are affected by the same spatial and temporal variations as are the comparisons of the correlative data with GPS/MET data.

Comparisons are based on a set of about 280 radiosonde and GPS/MET matches. The smaller number of comparisons at low elevations is due to radiosondes launched from higher elevations. The decrease in number above 15 km is due to the fact that radiosonde balloons burst at different altitudes ranging from 15 to 30 km. As shown in Plates 5 and 6, the NCEP and ECMWF data agree with radiosonde data, on average, within 1% in refractivity and 1°C in temperature, except near the top of the soundings where differences are greater. The standard deviation of the radiosonde and the analyses temperature differences is about 2°C. The refractivity standard deviation is typically 2%, but can reach 4% in the lower troposphere. Part of this discrepancy is due to the spatial and temporal decorrelation.

The excellent agreement between the radiosonde data and the analyses is expected because the radiosonde data, where they exist, are the dominant observations affecting the analysis.

5.2.3. Comparison of NCEP analyses with MLS, TOVS and GOES data. For comparison of MLS and NCEP data, only those MLS soundings that also have matching GPS/MET soundings within the specified spatial and temporal window are used. MLS pressures are mapped to geometric altitudes by using the NCEP relationship between pressure and height. For comparison of low vertical resolution data such as MLS with higher resolution data, we use a binning method. The bins, representing atmospheric layers, bracket the lower resolution data. The higher resolution data are interpolated to the levels of the lower resolution data within each bin. We use linear interpolation for temperature and log-linear interpolation for refractivity, which changes exponentially with height. Each pair of values is then differenced in the appropriate bin. Average, standard error of the mean, and standard deviations are computed for all differences within a bin.

As shown in Plate 7, the NCEP and MLS data agree on average to better than 1% in refractivity with a standard deviation of 1 to 2% for the entire comparison range. The mean temperature differences are less than 2°C with a standard deviation of 3 to 4°C.

A binned comparison of NCEP and TOVS soundings is shown in Plate 8. There is agreement in N to within 1% with a 1% standard deviation. Mean temperature agreement is better than 1°C from 14 km to almost 40 km. Above this altitude, TOVS shows a negative bias of up to 5°C relative to NCEP. We believe that this bias is caused by the low resolution of TOVS near the stratopause. Temperature standard deviation ranges from 2°C at 15 km to 3°C at 50 km.

The final temperature and refractivity comparisons between correlative data are shown for NCEP and GOES-8 soundings. This comparison is done at the locations where GOES and GPS/MET profiles coincide. GOES-8 covers only approximately 3% of the Earth and thus only 3% of the GPS/MET occultations fell within the GOES 8 field of view. Therefore, only 32 GOES and GPS/MET matches were found.

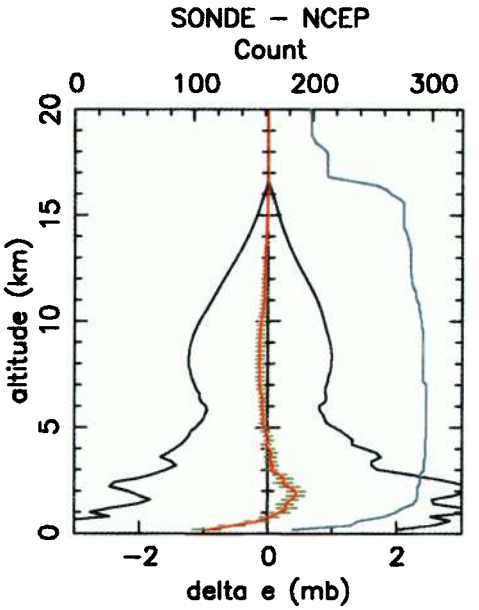

Plate 17. Radiosonde minus NCEP water vapor profiles at GPS/MET locations and times.

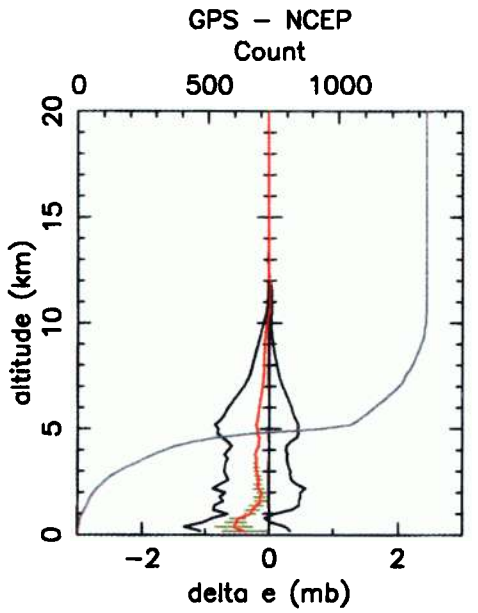

Plate 18. GPS/MET minus NCEP water vapor profiles at GPS/MET locations and times.

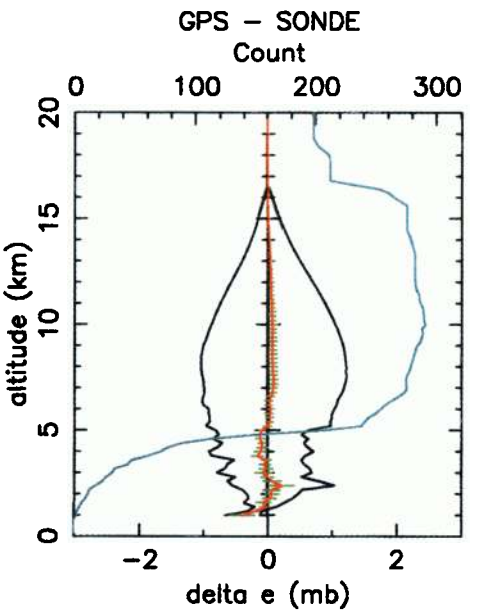

Plate 19. GPS/MET minus radiosonde water vapor profiles at GPS/MET locations and times.

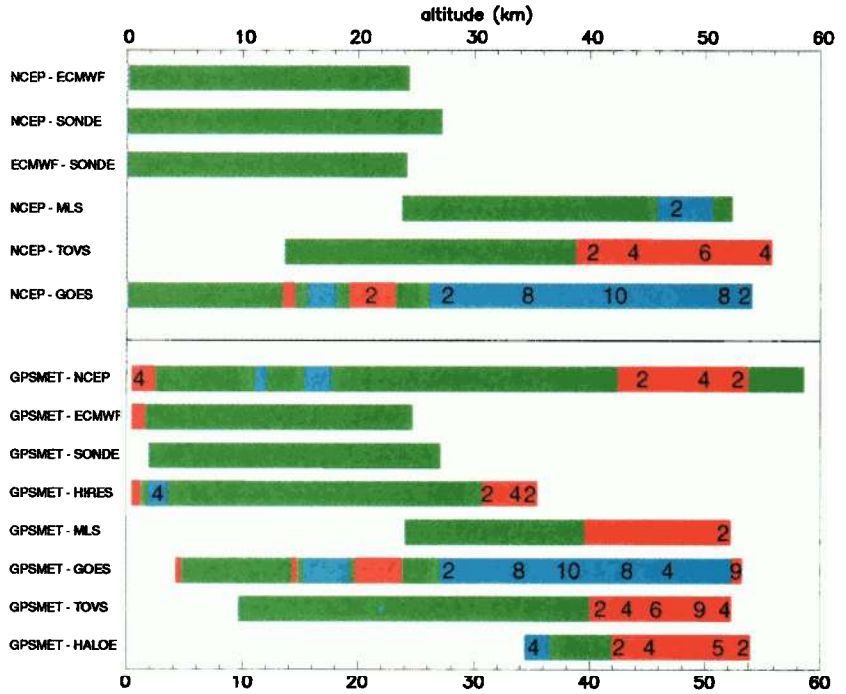

Plate 20. Summary of temperature comparison statistics. The upper six bars compare correlative temperatures, and the lower eight bars compare GPS/MET dry temperature to correlative dry temperatures. The data sources compared are labeled on the left. Colored bars indicate altitude intervals of the comparisons. Regions where average temperatures agree within ±1°C are indicated in green, positive differences greater than 1°C are in red, and negative differences less than -1°C are in blue. The magnitude of temperature differences (°C) is labeled where it occurs.

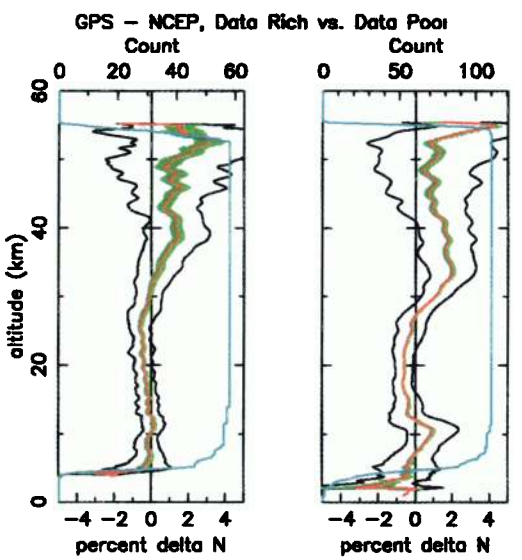

Plate 21. GPS/MET minus NCEP refractivity profiles for data rich (left panel) and data poor (right panel) regions.

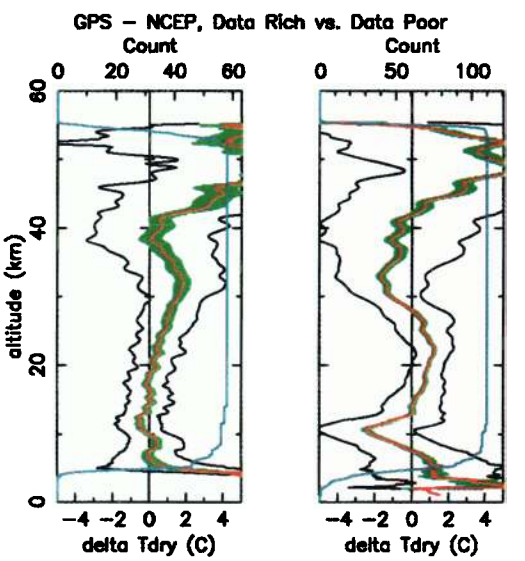

Plate 22. GPS/MET minus NCEP dry temperature profiles for data rich (left panel) and data poor (right panel) regions.

Plate 9 shows good average agreement between GOES and NCEP refractivity (1% to 2%) and temperature (1°C to 2°C) from the surface to about 25 km. The standard deviation of refractivity is about 4% near the surface and less than 1% at 25 km. The standard deviation of the temperature difference is about 2°C from 1 to 25 km. The bends in the temperature comparison between 12 and 18 km are caused by a few large differences in this relatively small sample of comparisons. GOES profiles above 25 km develop a large warm bias compared to the NCEP analyses.

It should be noted once again that all comparisons between NCEP and correlative data are affected by temporal and spatial decorrelation because the gridded data are interpolated to GPS/MET locations and times. The NCEP and ECMWF comparison is not affected in this way because both analyses are interpolated to GPS/MET locations.

5.3. Comparison of Correlative Data With GPS/MET Data

GPS/MET refractivity can be compared directly with refractivity computed from correlative pressure, temperature and water vapor profiles. Similarly GPS/MET temperatures can be compared directly to correlative temperatures above levels where water vapor is present in significant amounts.

As discussed earlier and illustrated in Plate 2, in layers where water vapor is present in significant amounts, it is possible to compute an estimate (termed T_{wet}) of the actual temperature using the observed refractivity and an independent estimate of water vapor pressure. Because new data types are best validated and used without attempting to transform them to traditional variables (like T_{wet}) (E. Kalnay, personal communication, 1997), we compute refractivities and dry temperatures from the correlative data sets for comparison.

After refractivity for the correlative data is computed from equation (1), "dry pressure" is determined by assuming that this refractivity is a function of dry air density only. It can be seen from equation (1) that dry pressure is higher than total pressure when water vapor is present. Dry temperature is then computed from refractivity and dry pressure under the assumption that no water vapor is present. This dry correlative temperature is lower than actual temperature, but it can be compared directly to GPS/MET dry temperatures.

We emphasize once again that GPS/MET refractivity need not be converted to temperature for assimilation into models. The process described here is for the sole purpose of validation and comparison.

5.3.1. Comparison of GPS/MET data with NCEP and ECMWF analyses. NCEP and ECMWF model data are interpolated to the location of each occultation as described in the previous section. The statistical results of these comparisons are shown in Plates 10 and 11.

The GPS/MET and NCEP refractivities agree on average to within 1% from 1 to 50 km. The standard deviation ranges between 1 to 2% in the height range from 1 to 30 km. Above 30 km, the standard deviation increases in large part due to higher vertical resolution (Plates 1 and 2) of the GPS/MET soundings which contain temperature fluctuations that are not present in the analyses.

The average temperature agreement between GPS/MET and NCEP is within 1°C from 1 to 42 km. The dry temperature standard deviation is approximately 2°C from 10 to 25 km, but increases below 10 km and above 25 km. The increase in dry temperature standard deviation in the lowest 10 km is due to the variable distribution of water vapor. The increase above 25 km is caused by the wavelike structure in temperature and the higher vertical resolution of the GPS/MET data.

As shown by additional comparisons discussed later in this paper, we believe that the cold bias of NCEP relative to GPS/MET temperature above approximately 48 km is an error in the analysis caused by the strong influence of TOVS data on the NCEP analysis at these altitudes.

We see a slight warm bias in NCEP relative to GPS/MET between 10 and 20 km. Because the GPS/MET soundings resolve the temperature minimum at the tropopause better than the NCEP analysis (Plate 1), the NCEP soundings appear warmer on the average in this region. High resolution in the vicinity of the tropopause is important for resolving features near the tropopause (such as potential vorticity maxima) which are related to upper level fronts, cyclogenesis, tropopause folds and stratospheric-tropospheric exchange processes [*Davis and Emanuel*, 1991], and is an important strength of the GPS/MET occultation technique.

Below 6 km the number of comparisons drops sharply because fewer GPS/MET soundings penetrate the lowest troposphere due to antenna gain limitations. A cutoff was applied in the first instance that the signal-to-noise ratio dropped below 60 volt per volt (v/v) at an altitude below 5 km to avoid corrupted GPS/MET data from entering the statistics.

Comparison of the GPS/MET and ECMWF soundings in Plate 11 confirms what is shown for the NCEP comparisons. Below 8 km the agreement between ECMWF and GPS/MET refractivities is slightly better than the agreement between NCEP and GPS/MET refractivities, which suggests that ECMWF water vapor agrees better with GPS/MET than does the NCEP water vapor. Between 1 and 8 km, GPS/MET dry temperatures also compare slightly better with ECMWF than with NCEP temperatures. The slight warm bias that was seen in the GPS/NCEP comparison between 10 and 20 km is not seen here, indicating better resolution of the tropopause in the ECMWF analyses compared to the NCEP analyses (Plate 1).

5.3.2. Comparison of GPS/MET and radiosonde data. For comparison of GPS/MET and radiosonde data, we used radiosonde soundings that were close in time and space as explained above. We computed refractivity and dry temperatures from the interpolated sonde data and interpolated these profiles to the 200 m resolution of the GPS/MET data.

As shown in Plate 12, the mean difference between GPS/MET and radiosonde refractivities agrees to within 1% with 1 to 2% standard deviation from 2 to 25 km. The average difference of the dry temperatures agrees to better than 0.5°C from 2 to 28 km, with a standard deviation of 2 to 3°C above 10 km. Below 10 km the standard deviation of the dry temperature difference increases because of the variability of water vapor. The drop in the number of correlative radiosondes above 15 km is due to a decreasing number of radiosondes that provide data above that altitude. The drop in comparisons below 6 km is primarily due to the smaller number of GPS/MET soundings that penetrate the atmosphere down to the surface.

5.3.3. Comparison of GPS/MET and MLS, GOES, TOVS, and HALOE data. For comparison with MLS data, GPS/MET observations were binned within specified layers containing the lower resolution MLS observations. Plate 13 shows comparisons at the midpoints of the seven discrete layers for which MLS data are available. Note that GPS/MET data above 50 km are weighted increasingly by climatology because of decreasing signal to noise ratios at high altitudes.

Plate 13 shows very good agreement on the average for refractivity and temperature from 24 to 45 km. The mean temperatures differ by 1 to 2°C for the entire range of MLS data up to 52 km. GPS and MLS temperatures agree on average better than NCEP

and MLS temperatures, and below 30 km the standard deviation of the GPS and MLS comparison is also slightly smaller. The temperature standard deviation increases with altitude, again due to the high-frequency temperature fluctuations in the GPS/MET data above 30 km.

The comparison with GOES data, shown in Plate 14, is limited to the relatively small sample of 32 GPS/MET profiles that fell within the GOES field of view during the test period.

Agreement with average GOES refractivity is of the order of 1% from 4 to 20 km, with a standard deviation of 1 to 2% between 10 km and 20 km and 2 to 3% between 10 and 4 km. Dry temperatures agree on average within 1 to 2°C from 4 to 10 km with standard deviations of 3 to 4°C. GOES and GPS/MET data do not agree well above 25 km, with GOES data showing a large warm bias in this region. Standard deviations increase in the lower troposphere because of water vapor variability.

Almost every GPS/MET sounding could be matched with a TOVS sounding because of the excellent TOVS global coverage. TOVS temperature data were available at 15 pressure levels from 922 to 0.6 mbar. TOVS moisture data were only available for three levels and were not used for this study. Because high-resolution moisture data were not available for TOVS, temperature comparisons were only completed above 10 km.

As shown in Plate 15, GPS/MET and TOVS refractivities agree on average to within 1% from 10 to 44 km with standard deviations of 1 to 2% from 10 to 30 km. The temperatures agree to within 1°C from 10 to 40 km on average, with a 2°C standard deviation. TOVS has a significant (up to 9°C) cold bias as compared to GPS/MET above 40 km, probably due to TOVS' lower resolution of the temperature maximum at the stratopause.

Comparison of GPS/MET and HALOE soundings, shown in Plate 16 is based on 31 matching soundings, a relatively small number. HALOE data below 35 km are essentially equal to the NCEP analysis, and hence we show the comparison data only above 35 km. Because GPS/MET results are influenced by climatology above 50 km, an independent comparison between the two instruments is possible only between 35 and approximately 50 km.

Average GPS/MET and HALOE refractivities agree to about 1 to 2%, with 2 to 3% standard deviation from 35 to 45 km. Temperature agreement is 1 to 2°C up to about 40 km where a several degree cold bias of HALOE relative to GPS/MET develops. This cold bias reaches 5°C at 50 km and is believed to be an error in the HALOE data, again because the GPS/MET and MLS data agree very well here.

5.4. Water Vapor Comparisons

GPS/MET water vapor profiles were computed as explained in section 2.2.3 and compared to water vapor computed from the NCEP analyses and from nearby radiosondes.

Here again, we computed the NCEP profiles for the times and locations of the GPS/MET soundings that occurred within the specified temporal and spatial match criteria. We then compared the NCEP water vapor profiles with the nearby radiosondes that were used for the GPS/MET comparisons (Plate 17). Therefore the NCEP and radiosonde comparisons are affected by the high degree of temporal and spatial decorrelation of water vapor.

The vapor pressures from NCEP and the radiosondes agree in the mean within 0.5 mbar above 1 km, with standard deviations of more than 2 mbar in the lowest levels, decreasing with increasing elevation (Plate 17).

Plate 18 shows that NCEP and GPS/MET average water vapor pressures agree to better than 0.5 mbar down to an altitude of 1 km. While the comparison below 5 km is based on a decreasing number of the GPS/MET soundings, the standard deviation is 0.5 to 1 mbar nearly all the way to the surface. There are two reasons why GPS/MET and NCEP water vapor pressures agree better than the radiosonde and NCEP water vapor pressures. First, only a few GPS/MET soundings penetrate below 5 km, and those that do generally occur in regions of lower water vapor. Second, the gridded data are interpolated to the GPS/MET location whereas radiosonde data are not co-located with GPS/MET data.

Plate 19 shows very good agreement (better than 0.3 mbar) between average GPS/MET and radiosonde water vapor pressures above 1 km. The standard deviation at 3 km is about 0.5 mbar. Again, statistics at 3 km are based on a small number of only about 50 comparisons. This good agreement is aided by the fact that most GPS/MET occultations that penetrate to near the ground with sufficient signal strength occur in relatively dry atmospheres without large water vapor gradients.

6. Interpretation of Statistics

Statistical comparisons between correlative data, and between GPS/MET and correlative data, are summarized in Plate 20. Average temperature agreement within ±1°C is shown in green; warmer and cooler differences are shown in red and blue. The magnitude of temperature differences is labeled where it occurs.

The combined statistical comparisons of GPS/MET with radiosondes, MLS, HALOE, and TOVS demonstrate that GPS/MET temperatures between 1 and 40 km agree on average to within 1°C with the most accurate of the other systems. From 40 to 50 km TOVS, HALOE and NCEP display a several degree cold bias relative to GPS/MET with the maximum cold bias around 50 km, which is the mean altitude of the stratopause (Figure 1). MLS shows a much smaller cold bias in this region and agrees within 1 to 2°C with GPS/MET.

Because of the agreement with MLS, the strong influence of TOVS on NCEP, the published stratospheric cold bias of HALOE, and the theoretically expected performance of GPS/MET in the 10 to 50 km height range, we believe that GPS/MET temperatures over this entire range are accurate, on average, to about 1°C. The temperature fluctuations in the GPS/MET soundings between 30 and 50 km affect the comparison statistics by increasing the standard deviations. These fluctuations have not, at present, been verified and remain the subject of ongoing investigations.

The GOES soundings show a large warm bias relative to GPS/MET between 28 and 50 km, with a maximum warm bias of 10°C at 40 km. Because of the good agreement among the NCEP, MLS, TOVS, and GPS/MET data at this level, we believe the GOES retrievals are in error in this region.

In the troposphere the GPS/MET average dry temperatures and refractivities agree very well with ECMWF data down to an altitude of 1 km. From 8 km to 1 km, GPS/MET average refractivity agrees slightly better with ECMWF and radiosondes than with NCEP data. Thus our statistics suggest that the ECMWF water vapor analyses may be more accurate than the NCEP analyses. Refractivity comparison with the global analyses, radiosondes, and GOES data shows average agreement of better than 1% in refractivity from 1 km upward to 25 km. Standard deviations of these differences are comparable to those between correlative data and the NCEP model.

6.1. Retrieval Difficulty in the Lower Troposphere

In the lowest part of the troposphere, GPS/MET refractivity data are often biased significantly toward lower values than the correlative data. These cases of N bias can generally be identified by a low signal to noise ratio (SNR) data cutoff. A low SNR cutoff of 60 v/v was applied to the data used in the statistical analysis. Only a subset of the soundings that penetrate close to the surface are biased. The N bias is strong for moist tropical occultations and barely noticeable for dry polar occultations. Thus the bias is believed to be related to sharp vertical gradients in atmospheric refractivity due to sudden changes in water vapor. We investigated the GPS instrument performance during rapid phase changes, atmospheric superrefraction and subrefraction, possible errors in the equation for refractivity, ionospheric conditions, occultation geometry, and other aspects of the retrieval process for possible causes of this bias. At present we believe that the most likely reason causing the negative N bias may be subrefraction in the moist troposphere occurring in thin layers with positive vertical gradients of refractivity $dN/dz > 0$. This hypothesis needs to be investigated in more detail.

It is clear, however, that this bias occurs only in the lowest part of the troposphere when the carriers are tracked at very low signal strength. Future instruments will employ more sophisticated tracking loops and higher gain antennas, resulting in SNR improvements over the current proof-of-concept mission by a factor of 3 (T. Meehan, personal communication, 1997). These advances should make it possible to track a significantly higher portion of occultations to Earth's surface. While it is important to understand the reasons for the N bias prior to launching future GPS/MET missions, we believe that a significantly smaller fraction of occultations will be affected when improved hardware is used.

6.2. Regional Comparisons

Statistical comparisons are useful to validate the GPS/MET data, but they do not fully demonstrate the potential benefits of this new technique for numerical weather prediction. Ideally this should be done with impact studies using actual data. However, 150 soundings in 24 hours distributed over the entire Earth do not provide sufficient data density for meaningful impact studies. Further insight into the potential impact of a future GPS/MET constellation may be obtained by comparing GPS/MET data with NCEP analyses in data rich and data sparse regions. If the GPS/MET data agree better with the analyses in the data rich region, it is likely that GPS/MET data assimilation would improve the overall global analyses, because there is no reason to believe that GPS/MET data quality is different for the two regions.

Plates 21 and 22 compare refractivity and dry temperatures over the continental United States and Europe (data rich regions) with the South Pacific (data sparse region).

Both figures illustrate that GPS/MET and NCEP agree better in refractivity and in temperature in the data rich region than in the data sparse region. Thus we conclude that the availability of operational quality GPS/MET profiles could lead to improvements in model fields. These results support the findings of *Leroy* [1997], who showed that upper tropospheric geopotential height fields computed from GPS/MET data agreed quite closely with ECMWF analyzed heights over data rich regions but departed strongly over the data sparse region of the Southeast Pacific.

7. Scientific Uses of the Data

High-resolution global observations of refractivity could be useful in climate studies by providing accurate temperature data above approximately 7 km and useful estimates of water vapor below this level when a reasonably accurate independent estimate of temperature is available. However, the most powerful use of radio occultation data is likely to be in the direct assimilation of the more fundamental observations and derived products, such as refractivity, or even bending angle in high resolution global weather prediction models, rather than trying to separate out temperature and water vapor from the refractivities [*Eyre*, 1994; *Zou et al.*, 1995; *Hoeg et al.*, 1996]. *Kuo et al.* [1997a] show that the assimilation of refractivity in a numerical model causes the temperature, winds, and water vapor fields to adjust in a mutually consistent way, leading to a more accurate prediction of an intense cyclone. Thus there are good reasons to expect that a dense set of refractivity observations from a constellation of LEO satellites, when continuously assimilated into global models, would produce significant improvements in the global analyses of temperature, winds and water vapor.

GPS/MET observations are complementary to other observational systems. The potential strengths of GPS limb soundings include the following.

1. They can provide global and roughly evenly distributed coverage at relatively low cost.
2. They are not significantly affected by clouds, precipitation or aerosols.
3. They have high vertical resolution (ranging from 0.1-0.5 km in the troposphere to 1.5 km in the stratosphere).
4. They require no first-guess fields and are one of the few upper air measurement systems that are completely independent of radiosonde data.
5. They are "self-calibrating" and have no instrument drift because the basic carrier phase observations are based on time measurements. Thus data from different satellites may be used without need for intercalibration.

Potential limitations of the radio occultation technique include the following.

1. The relatively long horizontal scale (approximately 300 km) of a single observation along the path of the ray may limit the usefulness of the observation for resolving fine-scale atmospheric features.
2. Like all of the satellite-based sounding data examined in this report, the GPS/MET observations provide no direct information on winds.
3. Reliable GPS/MET retrievals to Earth's surface in regions of significant water vapor have yet to be demonstrated.

For climate studies the long horizontal length scale may not be a serious problem; indeed the averaging out of small-scale features may be an advantage. In addition, with several LEO satellites in orbit, it will be possible to reduce this length scale to 200 km or less using tomographic techniques. It is also possible to assimilate the relatively large scale radio occultation measurements in models while preserving the strong horizontal gradients in the models.

The limited penetration and related negative N bias problem appears to be the most serious shortcoming at this time and must be fully understood prior to launching a future GPS/MET constellation. Hardware improvements at JPL and software development and research with the GPS/MET database at UCAR are currently under way to address this shortcoming.

While the single satellite proof-of-concept GPS/MET mission has validated and advanced the occultation technology, its observations are of limited value for weather prediction and impact studies because of the relatively low density of the observations in space and time. There is considerable interest in further demonstration of the value of GPS/MET observations for weather prediction and at-

mospheric research. Several international GPS occultation experiments are scheduled to be launched in the next 2 years. In addition, constellations of GPS occultation satellites have been proposed by public and private groups. An eight satellite constellation could provide 4000 daily soundings to operational centers within hours of real time.

Acknowledgments. The GPS/MET program is sponsored primarily by the National Science Foundation (NSF) with additional funding provided by the Federal Aviation Administration (FAA) and the National Oceanic and Atmospheric Administration (NOAA). In addition, the National Aeronautics and Space Administration (NASA) is providing funding directly to the Jet Propulsion Laboratory (JPL) for support of GPS/MET. The authors thank Kevin Trenberth and Bill Bonner from the National Center for Atmospheric Research (NCAR), Jim Yoe (NOAA/NESDIS) and Mel Gelman (NOAA/NCEP), and three anonymous reviewers for corrections and suggestions that greatly improved this paper.

References

Ahnert, P. R., Precision and Comparability of National Weather Service upper air measurements, paper presented at the *7th Symposium on Meteorological Observations and Instruments*, Am. Meteorol. Soc., New Orleans, La., 1991.

Anthes, R. A., *Meteorology*, 7th ed., 214 pp., Prentice-Hall, Englewood Cliffs, N.J., 1997.

Davis, C. A., and K. A. Emanuel, Potential vorticity diagnostics of cyclogenesis, *Mon. Weather Rev.*, *119*, 1929-1953, 1991.

Deutsches Klimarechenzentrum, The ECHAM3 Atmospheric General Circulation Model, *Tech. Rep. 6*, Hamburg, 1994.

Elliot, W. P., and D. J. Gaffen, On the utility of radiosonde humidity archives for climate studies. *Bull. Am. Meteorol. Soc., 72*, 1507-1520, 1991.

Eyre, J., Assimilation of radio occultation measurements into a numerical weather prediction system, *Tech. Memo. 199*, Eur. Cent. for Medium Range Weather Forecasts, *Reading, England*, 1994.

Fishbein, E. F., et al., Validation of UARS Microwave Limb Sounder temperature and pressure measurements, *J. Geophys. Res., 101*, 9983-10,016, 1996.

Fjeldbo, G., A. J. Kliore, and V. L. Von Eshelman, The neutral atmosphere of Venus as studied with the Mariner V radio occultation experiments, *Astron. J., 76*, 123-140, 1971.

Gelman, M. E., A.J. Miller, R.N. Nagatani, and C.S. Long, Use of UARS data in the NOAA stratospheric monitoring program, *Adv. Space Res.*, 14(9), 921-931, 1994.

Gorbunov, M., and S. Sokolovskiy, Remote sensing of refractivity from space for global observations of atmospheric parameters, *Rep. 119*, 58 pp. Max Planck Inst. for Meteorol., Hamburg, Germany, 1993.

Gorbunov, M., S. Sokolovskiy, and L. Bengtsson, Space refractive tomography of the atmosphere: Modeling of direct and inverse problems, *Rep. 210*, Max Planck Inst. for Meteorol., Hamburg, Germany, 1996.

Gurvich, A. S., and S. V. Sokolovskiy, Reconstruction of a pressure field by remote refractometry from space, *Izv. Acad. Sci. USSR Atmos. Oceanic Phys., Engl. Transl., 21*, 7-13, 1985.

Hayden, C. M., GOES VAS simultaneous temperature-moisture retrieval algorithm, *J. Appl. Meteorol., 27*, 705-733, 1988.

Hocke K., Inversion of GPS meteorology data, *Ann. Geophys.*, 15, 443-450, 1997.

Hoeg, P., A. Hauchecorne, G. Kirchengast, S. Syndergaard, B. Belloul, R. Leitinger, and W. Rothleitner, Derivation of atmospheric properties using a radio occultation technique, Sci. Rep., *95-4*, Danish Meteorol. Inst., 1996.

Kalnay, E., et al., The NCEP/NCAR 40-year reanalysis project, *Bull. Am. Meteorol. Soc., 77*, 437-471, 1996.

Karayel, E. T., and D. P. Hinson, Sub-Fresnel-scale vertical resolution in atmospheric profiles from radio occultation, *Radio Sci., 32*, 411-423, 1997.

Kuo, Y.-H., X. Zou, and W. Huang, The impact of GPS data on the prediction of an extratropical cyclone: An observing system simulation experiment, *J. Dyn. Atmos. Ocean*, in press, 1997a.

Kuo, Y.-H., X. Zou, S.-J. Chen, W. Huang, Y.-R. Guo, R. Anthes, M. Exner, D. Hunt, C. Rocken, and S. Sokolovskiy, A GPS/MET sounding through an intense upper-level front, *Bull. Am. Meteorol. Soc.*, in press, 1997b.

Kursinski, R., et al., Initial results of radio occultation observations of earth's atmosphere using the Global Positioning System, *Science, 271*, 1107-1110, 1996.

Leroy, S., The measurement of geopotential heights by GPS radio occultation, *J. Geophys. Res., 102*, 6971-6986, 1997.

Luers, J. K., and R. E. Eskridge, Temperature corrections for the VIZ and Vaisala radiosondes, *J. Appl. Meteorol., 34*, 1241-1253, 1995.

Melbourne, W., E. Davis, C. Duncan, G. Hajj, K. Hardy, E. Kursinski, T. Meehan, L. Young, and T. Yunck, The application of space borne GPS to atmospheric limb sounding and global change monitoring, *JPL Publ., 94-18*, 147 pp., 1994.

Menzel, W. P., and J. F. V. Purdom, Introducing GOES-I: The first of a new generation of geostationary operation environmental satellites, *Bull. Am. Meteorol. Soc., 75*, 757-781, 1994.

Nash, J., and F. J. Schmidlin, WMO international radiosonde comparison, instruments and observing methods, *Rep. 30, WMO/TD-No. 195*, 103 pp., World Meteorol. Organ., Geneva, 1987.

Neilan, R., The evolution of the IGS global network, current status and future prospects, International GPS Service for Geodynamics, 1994 Annual Report, *JPL Publ., 95-18*, 25-34, 1995.

NOAA, *Strategic Plan for Upper Air Observations*, 18 pp., Silver Springs, Md., 1992.

Phinney, R. A., and D. L. Anderson, On the radio occultation technique for studying planetary atmospheres, *J. Geophys. Res., 73*, 1819-1827, 1968.

Russell, J. M., III, L. L. Gordley, J. H. Park, S. R. Drayson, D. H. Hesketh, R. J. Cicerone, A. F. Tuck, J. E. Frederick, J. E. Harries, and P. J. Crutzen, The Halogen Occultation Experiment, *J. Geophys. Res., 98*, 10,777-10,797, 1993.

Russell, J. M., III, L. L. Gordley, L. E. Deaver, R. E. Thompson, and J. H. Park, An overview of the Halogen Occultation Experiment (HALOE) and preliminary results, *Adv. Space Res., 14*, 9-13, 1994.

Schmit, T. J., Sounder bias correction of the east-west gradient, paper presented at *GOES and Beyond, SPIE Conference*, Soc. Photo. Opt. Instrum. Eng., Denver, Colo., Aug. 4-9, 1996.

Schwartz, B. E., and C. A. Doswell, North American rawinsonde observations: Problems, concerns, and a call to action, *Bull. Am. Meteorol. Soc., 72*, 1885-1896, 1991.

Shea, D. J., S. J. Wifley, I. R. Stern and T. J. Hoar, An introduction to atmospheric and oceanographic data, *NCAR Tech. Note, TN - 4044 IA*, 132 pp., 1994.

Smith, E. K., and S. Weintraub, The constants in the equation for atmospheric refractive index at radio frequencies, *J. Res. Natl. Bur. Stand., 50*, 39-41, 1953.

Smith, W. L., W. M. Woolf, C. M. Hayden, D. Q. Wark, and L. M. McMillan, The TIROS-N operational vertical sounder, *Bull. Am. Meteorol. Soc., 60*, 1177-1187, 1979.

Sokolovskiy, S., and D. Hunt, Statistical optimization approach for GPS/MET data inversions, paper presented at the URSI GPS/MET Workshop, Union Radio Sci. Int., Tuscon, Ariz., 1996.

Thayer, D., An improved equation for the radio refractive index of air, *Radio Sci., 9*, 803-807, 1974.

Theon, J., W. Nordberg, and L. Katchen, Some observations of the thermal behavior of the mesosphere, *J. Atmos. Sci., 24*, 428-438, 1967.

Trenberth, K.E., and C. J. Guillemot, Evaluation of the atmospheric moisture and hydrological cycle in the NCEP reanalysis, *NCAR Tech. Note, TN-430*, 308 pp., 1996.

Vincent, R. A., and I. M. Reid, HF Doppler measurements of mesospheric gravity wave momentum fluxes, *J. Atmos. Sci., 40*, 1321, 1983.

Vorob'ev, V. V., and T. G. Krasil'nikova, Estimation of the accuracy of the atmospheric refractive index recovery from Doppler shift measurements at frequencies used in the NAVSTAR system, *Phys. Atmos. Oceans, 29*, 602-609, 1994.

Ware, R., et al., GPS sounding of the atmosphere from low Earth orbit: Preliminary results, *Bull. Am. Meteorol. Soc., 77*, 19-40, 1996.

Wilson, R., A. Hauchecorne, and M-L. Chanin, Gravity wave spectra in the middle atmosphere as observed by Rayleigh Lidar, *Geophys. Res. Lett., 17*, 1585, 1990.

Zou, X., Y.-H. Kuo, and Y.-R. Guo, Assimilation of atmospheric radio refractivity using a nonhydrostatic mesoscale model, *Mon. Weather Rev., 123*, 2229-2249, 1995

R. Anthes, M. Exner, D. Hunt, C. Rocken, W. Schreiner, and R. Ware, University Corporation for Atmospheric Research, 3300 Mitchell Lane, Suite 393, PO Box 3000, Boulder, CO 80301. (e-mail: anthes@ucar.edu; exner@ucar.edu; dhunt@ucar.edu; rocken@ucar.edu; schrein@ucar.edu; ware@ucar.edu)

D. Feng and B. Herman, Department of Atmospheric Sciences, University of Arizona, Tucson, AZ 85721. (e-mail: feng@air.atmo.arizona.edu; herman@air.atmo.arizona.edu)

M. Gorbunov and S. Sokolovskiy, Russian Institute of Atmospheric Physics, Moscow, Russia. (e-mail: root@iaph.msk.su)

Y.-H. Kuo and X. Zou, National Center for Atmospheric Research, Boulder, CO 80307. (e-mail: kuo@ucar.edu; zou@ucar.edu)

(Received March 26, 1997; revised August 21, 1997; accepted August 25, 1997.)